Aluminum Basic Benzoate-Based Coatings: Evaluation of Anticorrosion Properties by Electrochemical Impedance Spectroscopy and Accelerated Tests

G. Blustein,[‡,] R. Romagnoli,[**] J.A. Jaén,[*] A.R. Di Sarli,[*] and B. del Amo[*]*

ABSTRACT

Insoluble metallic benzoates can be prepared from the corresponding soluble salts. Soluble benzoates can be used as inhibitors in neutral solutions while insoluble ones can be used as anticorrosive pigment for paints. This paper describes the experimental procedure to prepare aluminum basic benzoate ($AlC_{14}H_{11}O_5$) to be used in anticorrosive paints. The anticorrosive properties of aluminum basic benzoate were assessed by electrochemical techniques (corrosion potential and linear polarization measurements). The nature of the compounds forming the protective layer was determined using spectroscopic techniques (scanning electron microscopy/energy-dispersive x-ray microanalysis [SEM-EDAX], ultraviolet [UV]-visible diffuse reflectance, Fourier transform infrared [FTIR], and Mössbauer). In a second stage, the anticorrosive properties of the pigment were evaluated by incorporating it in alkyd and epoxy anticorrosive paints, which, in turn, were evaluated by accelerated (salt spray and humidity tests) and electrochemical measurements (electrochemical impedance spectroscopy). The morphology and the nature of the protective layer grown under the paint film in the salt spray chamber was assessed using SEM and UV-visible diffuse reflectance spectroscopy. Experimental results showed that basic aluminum benzoate was adequate to formulate solvent and water-borne epoxy anticorrosive paints with improved anticorrosive performance when it is used in combination with zinc oxide (ZnO). Zinc oxide counteracted the intrinsic acidity of basic aluminum benzoate. Solvent alkyd paints could also be prepared but with lower performance.

KEY WORDS: accelerated tests, aluminum basic benzoate, anticorrosive coatings, electrochemical tests

INTRODUCTION

Corrosion protection of metals and the need of improved environmentally benign surface coatings are high priority topics in the field of coatings technology. To date, steel corrosion inhibition has relied extensively on hexavalent chromium compounds included in both surface preparation and organic primers. However, the toxicity and carcinogenic properties of chromium has caused government agencies to impose severe restrictions on its use. Changing regulations dictate the use of fundamentally new coatings systems that are capable of meeting new environmental standards. In this sense, it is believed that benzoates as anticorrosive pigments for paints could match environmental concerns with proven anticorrosive efficiency.

The inhibitive properties of benzoate anion are well known and were studied using sodium benzoate ($C_7H_5NaO_2$) and benzoic acid ($C_7H_6O_2$) in different media, including those containing chloride.[1-15] The use of benzoate anion in combination with other anions such as gluconates was also reported,[16] and, more recently, the inhibitive properties of calcium benzoate ($CaC_{14}H_{10}O_4$) in neutral media were described.[17] Sodium benzoate and benzoic acid were used as corrosion inhibitors not only for ferrous substrates but also

Submitted for publication January 2007; in revised form, June 2007.

‡ Corresponding author. E-mail: pinturashigienicas@cidepint.gov.ar.

* CIDEPINT–Centro de Investigación y Desarrollo en Tecnología de Pinturas (CICPBACONICET), Calle 52 e/ 121 y 122 (B1900AYB), La Plata, Argentina.

** Departamento de Química Física, Facultad de Ciencias Naturales, Exactas y Tecnología, Universidad de Panamá, (0834-00900), Panamá, Panamá.

0010-9312/07/000163/$5.00+$0.50/0

for other metals such as aluminum,[18-22] zinc,[23-24] and copper.[25] The mechanism of the anticorrosive action of benzoates involves the adsorption of the anion on the anodic dissolution sites of the metallic surface, thus yielding an effective coverage that causes the corrosion rate to decrease.[16,26-27]

Soluble salts of benzoic acid were also used in concrete[28-29] and in the field of paint technology. In this last case, they were used as soluble inhibitive additives in anticorrosive coatings, and as active insoluble pigments in antifouling paints.[30-38]

The use of soluble compounds (benzoic acid, sodium benzoate, etc.) in anticorrosive paints is limited by the fact that their leaching by water penetrating the pores of the coating would greatly increase coating permeability with the concomitant loss of the protective properties of the paint. However, it is possible to prepare insoluble metallic benzoates with certain cations (zinc, iron, aluminum, etc.).

The objective of this investigation was to study the inhibitive properties of aluminum basic benzoate in paints. The pigment was precipitated under specific conditions and its anticorrosive properties were investigated by means of electrochemical techniques in pigment suspensions. In a second stage, anticorrosive paints containing aluminum basic benzoate were formulated and their performance was evaluated by accelerated (salt spray and humidity chambers) and electrochemical tests.

EXPERIMENTAL PROCEDURES

Pigment Preparation and Characterization

The solution-precipitate equilibrium between aluminum cation and benzoate anion was studied to find the most suitable conditions to precipitate an aluminum basic benzoate ($AlC_{14}H_{11}O_5$) and to determine its solubility. In this sense, the titration of each reactant (benzoic acid and aluminum ion) and the titration of a solution containing both ions, with standardized sodium hydroxide (NaOH), was carried out at constant temperature (25°C) in a thermostatized bath. The sodium hydroxide solution concentration was obtained by titration with potassium acid phthalate ($C_8H_5KO_4$).

The solubility product constant (K_{sp}) of aluminum hydroxide ($Al[OH]_3$) must be determined first to obtain K_{sp} of aluminum basic benzoate. This was accomplished by titrating 5.00 mL of 0.1019 M aluminum nitrate ($Al[NO_3]_3$), acidified with 15.00 mL of 0.1065 M hydrochloric acid (HCl), in the absence of sodium benzoate and in the presence of 75.00 mL of 0.0188 M sodium benzoate. The final volume in the titration cell was kept constant in all cases. The titration of benzoic acid was also carried out to obtain the acid constant in the reaction medium used in this research. The titrating solution was 0.1253 M NaOH. Reagent-grade chemicals were used in all cases and the working temperature was maintained at 25°C. In every case, stoichiometric constants were obtained and expressed in terms of the equilibrium concentrations of the different species.

As it will be discussed later, titration curves showed the advantage of preparing aluminum benzoate from 1.00 M ammonium benzoate and 0.33 M aluminum nitrate. The aluminum nitrate solution was dropped into the beaker containing 1 L of the benzoate solution, under continuous stirring. Once the addition of aluminum nitrate was completed, the solution was stirred for 1 h. The precipitate was washed three times with 10^{-3} M ammonium benzoate to avoid hydrolysis of the precipitate; the supernatant liquid was then decanted. Finally, the precipitate was filtered off by means of a Büchner funnel and dried at 50°C until constant weight.

The stoichiometry of the precipitate was determined weighing 0.2500 g of the precipitate and dissolving it in 180 mL of distilled water and 20 mL sulfuric acid (H_2SO_4) 1:1. The resulting solution was heated gently until complete dissolution was accomplished, cooled down to room temperature, and placed in a 250-mL volumetric flask. An aliquot of 10 mL was treated with 5 mL of 1.000 N potassium dichromate ($K_2Cr_2O_7$) plus 30 mL of concentrated H_2SO_4 and allowed to react 1 h at 50°C to determine the benzoate content in the precipitate. Then, 100 mL of distilled water was added to the beaker and the excess of potassium dichromate was back-titrated with 0.5000 N ferrous sulfate ($FeSO_4$) in a phosphoric medium, using a potentiometric technique with platinum electrodes polarized with 5 μA. Iron was determined by indirect gravimetry, weighting 1.0000 g of aluminum basic benzoate into a crucible. The sample was dried at 50°C and then burned at 1,100°C.

Physicochemical properties of the pigment, relevant to paint technology, such as density (ASTM D1475)[39] and oil absorption (ASTM D281),[40] were measured according to standardized procedures, to sketch a correct paint formulation.

The inhibitive properties of the anticorrosive pigment were evaluated by means of electrochemical techniques, using SAE 1010[(1)] (UNS G10100)[(2)] steel electrodes with 1.40 μm roughness. The corrosion potential was monitored as a function of time against a saturated calomel electrode (SCE) as reference. The supporting electrolyte was a pigment suspension in 0.025 M sodium perchlorate ($NaClO_4$). However, final tests on painted steel were carried out with both electrolytes. Electrochemical tests were also performed in suspensions containing zinc oxide, which was used to increase the pH of the aluminum benzoate suspension (3.58) to values for which the passivation of the

[(1)] Society of Automotive Engineers (SAE), 400 Commonwealth Dr., Warrendale, PA 15096.
[(2)] UNS numbers are listed in *Metals and Alloys in the Unified Numbering System*, published by the Society of Automotive Engineers (SAE International) and cosponsored by ASTM International.

substrate could be possible.[41] Zinc oxide is a pigment commonly added to paint formulations with certain anticorrosive properties.[42] Steel passivation starts at pH > 7,[41] but basic aluminum benzoate is acidic in nature while zinc oxide is basic. The addition of zinc oxide increased pH and generated a higher amount of benzoate ions as it may be deduced from equilibrium considerations. However, the action of zinc oxide is limited because the pH of its suspension is about 8.0. In addition, it was demonstrated that zinc salts polarize cathodic areas. That is to say, the slope of the I vs. E curve was diminished.

The morphology of the protective layer formed on steel, at the open-circuit potential, was studied using scanning electron microscopy (SEM) using a SEM coupled with energy-dispersive x-ray microanalysis (EDAX) (energy-dispersed form) to determine the surface elemental composition. The beam voltage was fixed at 15 kV. The surface composition obtained by EDAX analysis was semi-quantitative and was used to detect major and minor components of the protective layer. Previous results showed the advantage of obtaining spectra of the reaction products from a mix of spectroscopic pure iron and aluminum basic benzoate, in different proportions, which were wetted periodically with distilled water during a fortnight. The goal of this experience was to simulate the products that could be formed by a reaction between iron and aluminum basic benzoate, which could be responsible for the protection afforded by the pigment. Product identification was carried out through spectroscopic techniques: ultraviolet (UV)-visible diffuse reflectance, Fourier transform infrared (FTIR), and Mössbauer.

The reflectance spectra were recorded with a UV-visible spectrometer. Spectra were scanned in the 200-nm to 800-nm range at 50 nm/min. FTIR spectra were obtained using a spectrometer. The Mössbauer spectrometer was a conventional one of constant acceleration with a $^{57}Co(Rh)$ source of 20 mCi.

Steel corrosion rates, in pigment suspension in 0.5 M $NaClO_4$, were obtained from polarization curves. A SCE (E = 0.245 respect to the standard hydrogen electrode [SHE]) and a platinum grid were used as reference and counter electrodes, respectively. The swept amplitude was ±0.250 V from the open-circuit potential and the scan rate was 0.250 mV/s. Measurements were carried out with a potentiostat/galvanostat.

Paint Composition, Manufacture, and Application

Three different paints were formulated to carry out this research; two of them were solventborne (alkyd and epoxy) and the other was an epoxy waterborne paint.

The resins used to formulate solventborne paints were as follows: a bisphenol epoxy-polyamide resin (1:1 ratio v/v) and a medium oil alkyd (50% linseed oil, 30% o-phtalic anhydride, 8% pentaerythritol and glicerol, and 12% pentaerythritol resinate). The solvent used in the former case was a mixture xylene/methyl isobutyl ketone/butyl cellosolve (13/45/42%, by weight, w/w), while white spirit was used for the alkyd paint. The anticorrosive properties of the pigments were checked using solventborne paints because their behavior has been well documented for many years. The PVC/CPVC (pigment volume concentration/critical pigment volume concentration) relationship was 0.8 as suggested elsewhere.[43]

TABLE 1
Paint Composition

Components	Paints (vol%)		
	1	2	3
Aluminum basic benzoate	13.9	13.9	3.5
Barium sulfate	12.8	12.8	2.2
Talc	12.8	12.8	2.1
Titanium dioxide	5.1	5.1	2.1
Zinc oxide	1.2	1.2	0.3
Mica	—	—	1.8
Resin/hardener (1/1 ratio)	25.1	—	—
Alkyd resin	—	25.1	—
Resin/hardener (1/1.2 ratio)	—	—	65.8
Additives	—	—	1.5
Solvents	29.1	29.1	20.7

The anticorrosive pigment load was 30% v/v of the total pigment content; the same pigment content suggested when orthophosphates are used as anticorrosive pigments.[43-44] Titanium dioxide (TiO_2), barium sulfate ($BaSO_4$), and talc were incorporated to complete the pigment formula. All pigments were dispersed for 24 h in the vehicle, using a ball mill to achieve an acceptable dispersion degree.[45]

An epoxy resin, based on a mix of bisphenol A ($C_{15}H_{16}O_2$) and bisphenol F ($C_{13}H_{12}O_2$), was chosen to formulate waterborne paints. The curing agent (hardener), which also acts as an emulsifier, was a modified polyamidoamine with 50% of solids. The resin/hardener ratio was 100/120 w/w. Neutral demineralized water was used as the solvent.

The anticorrosive pigment content was 30% of the total pigment content, and titanium dioxide, barium sulfate, talc, and mica were incorporated to complete the pigment formula. Mica was added to the formulation because of its barrier properties and ability to reduce the "flash rusting" degree.[46] The PVC value, 25%, was chosen to enhance the barrier properties of the coatings. Paint composition is shown in Table 1.

SAE 1010 steel panels (15.0 by 7.5 by 0.2 cm) were sandblasted to Sa 2 1/2 (SIS 05 59 00),[47] degreased with toluene (C_7H_8), and then painted by brushing, to reach a dry film thickness of 80 ± 5 μm. Painted panels were kept indoors for 14 days before testing.

Evaluation of the Paint Anticorrosive Properties by Accelerated and Electrochemical Tests

For each type of paint, a set of three panels was placed in the salt spray chamber (ASTM B117).[48]

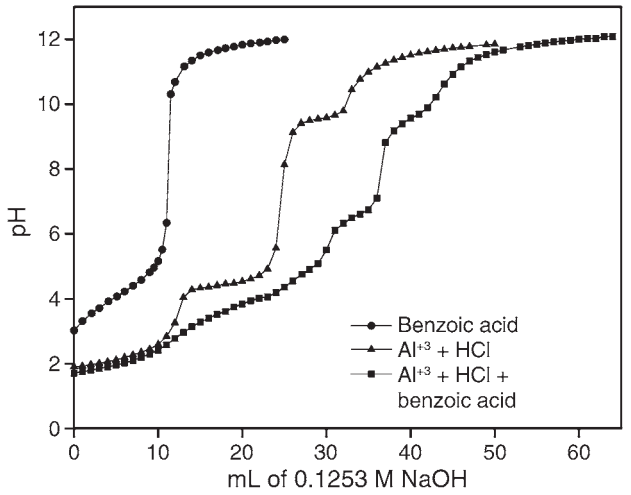

FIGURE 1. *Titration curves of different systems as a function of the volume of 0.1253 M NaOH.*

Rusting (ASTM D610)[49] and blistering (ASTM D714)[50] degrees were evaluated during 4,200 h of exposure. Wet adhesion was also determined according to the standard test (ASTM D3359, method B).[51]

The coating on the steel panels was removed, after the exposition to the salt spray chamber, using suitable solvents. The morphology of the protective layer on the metallic surface was observed by SEM, the surface elemental composition determined by EDAX, and, finally, corrosion products identified by UV-visible diffuse reflectance spectroscopy.

Another set of panels was placed in the humidity chamber, at 38 ± 1°C (ASTM D2247),[52] for 3,600 h. Rusting and blistering degrees were evaluated periodically, according to the above-mentioned standard specifications.

Impedance spectra of painted panels (frequency range: 1.10^5 Hz ≤ f ≤ 1.10^{-3} Hz) were performed in the potentiostatic mode, at the corrosion potential. Measurements were carried out as a function of the exposure time to the electrolyte solutions (0.5 M $NaClO_4$ and 3% sodium chloride [NaCl]), using a frequency response analyzer (FRA) and potentiostat. The amplitude of the applied alternating current (AC) voltage was 0.010 V peak-to-peak. Two acrylic tubes were attached to each coated panel (working electrode) with an epoxy adhesive to perform the electrochemical measurements. The geometric area exposed to the electrolyte in each cell was 15.9 cm^2. A large area Pt-Rh mesh of negligible impedance and SCE were used as auxiliary and reference electrodes, respectively. The experimental impedance spectra were interpreted on the basis of equivalent electrical circuits using a suitable fitting procedure developed by Boukamp.[53] These electrochemical experiments were carried out at laboratory temperature (20 ± 2°C) using a Faraday cage.

RESULTS AND DISCUSSION

Study of the Solution-Precipitate Equilibrium Between Aluminum and Benzoate Ions

The analysis of the precipitate, obtained when benzoate anion reacted with aluminum cation, revealed that there were two moles of benzoate (B) per each mole of aluminum cation; so it was concluded that the formula of the precipitate was AlB_2OH.

K_{sp} of aluminum hydroxide could be calculated as follows. Let V_1 be the volume used to titrate hydrochloric acid in the samples containing only aluminum cation (Figure 1), according to the equation:

$$H_3O^{1+} + OH^{1-} \rightarrow 2\ H_2O \qquad (1)$$

and V_2 is the volume of the base solution required to precipitate aluminum cation:

$$Al^{3+} + 3\ OH^{1-} \rightarrow Al(OH)_3 \downarrow \qquad (2)$$

The K_{sp} of aluminum hydroxide is defined by the expression:

$$K_{sp}\ [Al(OH)_3] = [Al^{3+}][OH^{1-}]^3 \qquad (3)$$

and calculated by the equation:

$$K_{sp}\ [Al(OH)_3] = \left[\frac{\frac{1}{3}(V_2 - V_a)M}{V_i + V_a}\right]\frac{K_W^3}{[H_3O^{1+}]^3} \qquad (4)$$

where V_a is the base volume corresponding, normally, to the middle point of the precipitation plateau of aluminum hydroxide and (V_i + V_a) is the total volume in the titration cell. From the experimental data in Figure 1, V_2 = 27.50 mL and the K_{sp} for aluminum hydroxide, calculated from the previous equation, equals 3.22×10^{-31}, being the value reported in the literature comprised between 1.22×10^{-30} and 1.26×10^{-33}.[54]

The precipitation curve of aluminum cation, in the presence of benzoic acid, did not show the typical shape corresponding to the precipitation of a unique compound (Figure 1). The curve was ill-defined up to 30.00 mL of titrating solution, and it seemed that two different compounds were formed. The low pH values recorded during the addition of 25.00 mL of base and the analysis of the precipitate suggested that aluminum basic benzoate coprecipitated with aluminum hydroxide.

The acid constant of benzoic acid was obtained from the titration curve of benzoic acid, following the procedure described in the literature.[54-55] The calculated value was 8.04×10^{-5}, very close to that reported by Wilson and Wilson, 6.30×10^{-5}.[54]

The equations for the dissociation of aluminum basic benzoate and the hydrolysis of the anion and

the cation are as follows. The constants associated with equilibrium are written and calculated below:

$$AlB_2OH \Leftrightarrow 2\ B^{1-} + Al^{3+} + OH^{1-} \quad (5)$$

$$K_{sp}[AlB_2OH] = [B^{1-}]^2[Al^{3+}][OH^{1-}] = \frac{K_{sp_{Al(OH)_3}}[B^{1-}]^2}{[OH^{1-}]^2} \quad (6)$$

$$B^{1-} + H_2O \Leftrightarrow HB + OH^{1-} \quad (7)$$

$$K^h_{B^{1-}} = \frac{[HB][OH^{1-}]}{[B^{1-}]} = \frac{K_W}{K_a} \Rightarrow K^h_{B^{1-}} = 1.24\times10^{-10} \quad (8)$$

where K_w is the ionic product constant of water at 25°C.

$$Al^{3+} + 6\ H_2O \Leftrightarrow Al(OH)_3 + 3\ H_3O^{1+} \quad (9)$$

$$K^h_{Al} = \frac{[H^{1+}]^3}{[Al^{3+}]} = \frac{[H^{1+}]^3[OH^{1-}]^3}{K_{sp_{Al(OH)_3}}} = \frac{K^3_W}{K_{sp_{Al(OH)_3}}} \Rightarrow K^h_{Al} = 3.11\times10^{-12} \quad (10)$$

The hydrolysis constant of the cation do not differ significantly from that of the anion and, as it was pointed out previously, aluminum basic benzoate was in equilibrium with aluminum hydroxide. As a consequence, K_{sp} of aluminum basic benzoate was calculated as follows:

$$K_{sp}[AlB_2OH] = [B^{1-}]^2[Al^{3+}][OH^{1-}] = \frac{K_{sp_{Al(OH)_3}}[B^{1-}]^2}{[OH^{1-}]^2} \quad (11)$$

The concentration of benzoate anion in equilibrium with the precipitated aluminum basic benzoate was obtained from 0.1019 M sodium benzoate solution to which the mili-moles of an aluminum cation, necessary to precipitate half of the amount of sodium benzoate, were added. Then, the final pH of the system (4.19) was measured, using a glass electrode, and this value was introduced in the preceding equation. The value of K_{sp} $[AlB_2OH] = 5.25 \times 10^{-15}$ was easily obtained and the solubility of the compound calculated. The theoretical solubility value was found to be 1.90×10^{-4} M (54.4 ppm) while the experimental value, obtained by indirect gravimetry, was 60.2 ppm.

Electrochemical Estimate of the Basic Aluminum Benzoate Anticorrosive Properties

The corrosion potential of the SAE 1010 steel electrode was displaced toward more negative values than those corresponding to the supporting electrolyte (Figure 2). This lack of passivity was attributed to the high acidity of the pigment suspension (pH = 3.58). Corrosion potential (E_{corr}) vs. time curve changed notably when zinc oxide was added to the pigment suspension, and potential values were much more positive and were still more positive than the values obtained with zinc oxide alone. This last fact suggested that together was a synergism between aluminum basic benzoate and zinc oxide, which rendered the electrode passivated. Zinc oxide not only polarizes the cathodic sites by precipitating sparingly soluble compounds[41] but it increases benzoate anion concentration raising the pH of the medium.

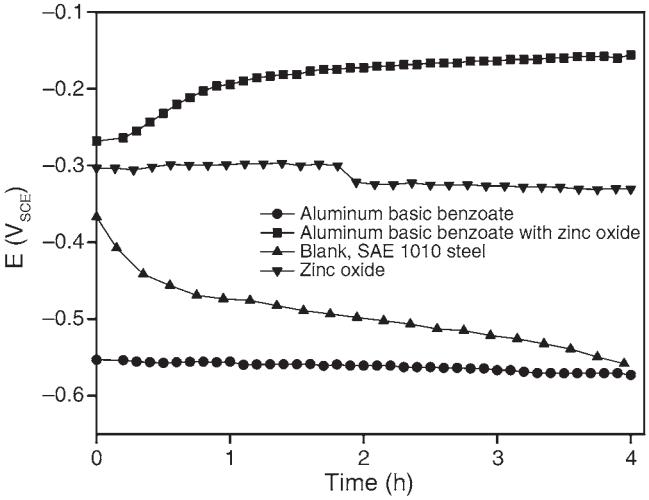

FIGURE 2. *Corrosion potential of SAE 1010 steel in aluminum basic benzoate/0.5 M $NaClO_4$ suspensions.*

The analysis of the polarization curve obtained after 3 h of exposure revealed the existence of high anodic currents and, as a consequence, poor protective properties. The cathodic current was also high, ~2.2 mA/cm^2. This rather high value suggested that oxygen reduction was overlapped with that of iron oxyhydroxides because the cathodic current density measured with a platinum electrode, in similar conditions, was 220 μA/cm^2 (Figure 3). So, it must be concluded that the steel electrode did not passivate in the suspension of aluminum basic benzoate. After 24 h of exposure, the situation did not change except that the cathodic current was a little lower.

The addition of zinc oxide to the suspension significantly changed the electrochemical behavior of steel. A peak, denoting passivity, appeared in the potential interval comprised between –0.450 V and –0.375 V. The cathodic current density decreased to 12 μA/cm^2 (Figure 3).

Corrosion rate, obtained from Tafel plots, was 2.14 mA/cm^2 after 3 h of exposure and 1.41 mA/cm^2 after one day had elapsed. In the presence of zinc oxide, the values were 2.94 μA/cm^2 (after 3 h) and 10.9 μA/cm^2 (after 24 h).

Zinc oxide by itself did not protect steel efficiently as it could be deduced from the polarization curves (Figure 3); it had some influence on the cathodic reaction because the current of this part of the polarization curve diminished after 24 h of exposure. No significant influence was observed in the anodic polarization branch. Zinc oxide reduced steel corrosion rate in supporting the electrolyte from 120 μA/cm^2 to

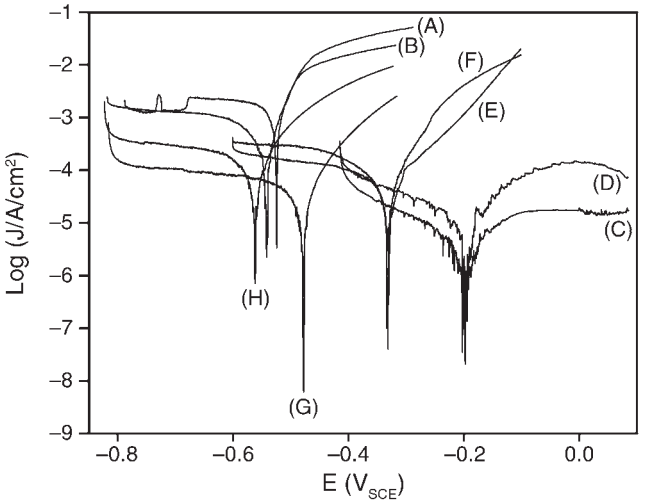

FIGURE 3. *Tafel plots of the SAE 1010 steel electrode in different media and exposure times: (A) aluminum basic benzoate, 3 h; (B) aluminum basic benzoate, 24 h; (C) aluminum basic benzoate + zinc oxide, 3 h; (D) aluminum basic benzoate + zinc oxide, 24 h; (E) zinc oxide, 3 h; (F) zinc oxide, 24 h; (G) blank, 3 h; and (H) blank, 24 h. In all cases the supporting electrolyte was 0.5 M $NaClO_4$.*

50.4 μA/cm² after 3 h and 142 μA/cm² to 65.6 μA/cm² after 24 h of exposure, respectively. However, as it was said previously, it was the combination of basic aluminum benzoate and zinc oxide that led to the lowest steel corrosion rates. The polarization curves obtained for aluminum basic benzoate + zinc oxide not only exhibited lower currents but they also displaced toward more positive potentials.

These facts led to the conclusion that aluminum basic benzoate could only inhibit corrosion in the presence of zinc oxide. For this reason, paints were formulated with this complementary pigment.

The protective layer, formed at the corrosion potential, was constituted by a uniform oxide film, constituted basically by iron oxides and oxyhydroxides (Figure 4[a]). A second layer, constituted by globular iron oxides, grew on the uniform layer. It was thought that these oxides had an expansive nature (Figure 4[b]). The uniform layer as well as the globular oxide contained low amounts of aluminum, 6.4% and 9.5%, respectively. The addition of zinc oxide to the suspension led to the formation of a more uniform film, which could exhibit better protective properties (Figure 4[c]).

Heterogeneous Reaction Between Pure Iron and Basic Aluminum Benzoate: Analysis of Corrosion Products

The nature of the corrosion products formed as a consequence of the heterogeneous reaction between a mix of spectroscopic pure iron and aluminum basic benzoate, in different proportions, was investigated using spectroscopic techniques, as it was said

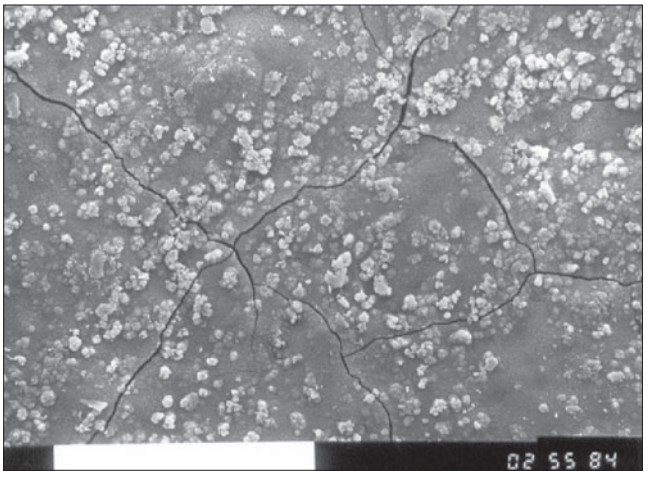

(a)

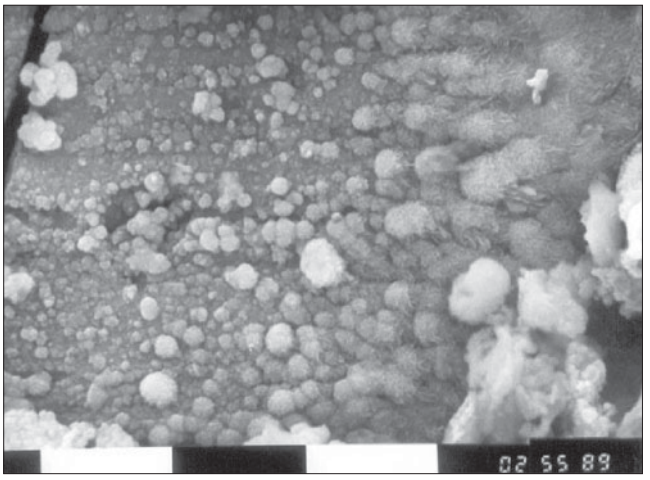

(b)

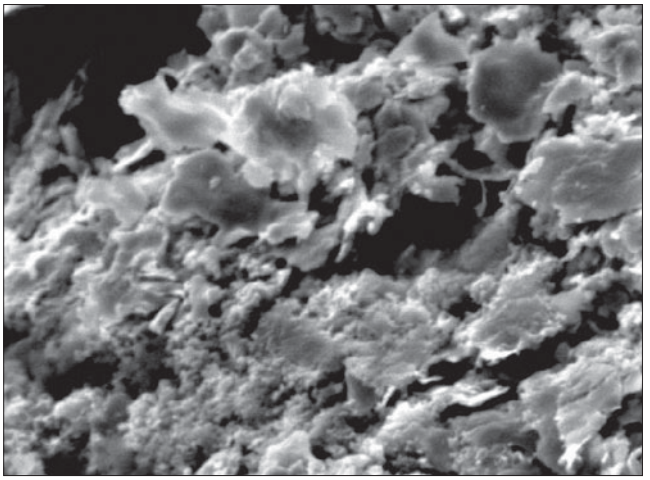

(c)

FIGURE 4. *SEM micrographs of the steel surface after being in contact for 24 h with aluminum basic benzoate/0.025 M $NaClO_4$ suspensions: (a) without zinc oxide (500X), (b) without zinc oxide (2,500X), and (c) with zinc oxide (2,500X).*

previously. UV-visible diffuse reflectance, FTIR, and Mössbauer spectra of aluminum basic benzoate, ferric benzoate, and ferric basic benzoate were obtained (Figure 5) for the sake of comparison because ferric benzoates could be formed during the corrosion reaction between iron and aluminum basic benzoate. The procedure used to obtain ferric benzoates was described elsewhere.[56] UV-visible spectra were deconvoluted by adjusting the spectral curve with multiple Gaussian peaks with commercial software. The fitting accuracy was assessed with the parameter χ^2, which was comprised between 1×10^{-5} to 4×10^{-5}. Band assignment for iron oxides and oxyhydroxides was carried out using the wavelength chart compiled by Larramona and Gutiérrez[57] and other spectroscopic studies reported in the literature.[58-59] Mössbauer spectra analysis was made by means of the Recoil program, using Lorentzian lines.

The UV-visible spectrum of ferric benzoate exhibited several important bands at 218 through 224, which are characteristic of benzoates: 274, 322, and 398 nm, respectively.[60] The most important bands of iron basic benzoate are located at 215, 287, and 371 nm. The UV-visible spectrum of aluminum basic benzoate only possesses two important bands at 218 nm and 274 nm. The FTIR spectrum of ferric benzoate exhibited, in the frequency group region, the following bands: 1,435, 1,493, 1,525, 1,564, 1,601, 1,687, 3,064, and 3,423 cm^{-1}. Ferric basic benzoate has a similar FTIR spectrum but it does not possess the bands located at 1,493, 1,566, and 1,674 cm^{-1}, the band at 1,674 cm^{-1} being the most intense band that could be used to differentiate both types of ferric benzoates. The FTIR spectrum of aluminum basic benzoate was quite similar to that of ferric benzoate but the band at 1,412 cm^{-1} was shifted to 1,635 cm^{-1}. The Mössbauer spectrum corresponding to either ferric benzoate or ferric basic benzoate had a central asymmetric doublet originated by a high spin ferric compound. The most characteristic Mössbauer parameters, isomer shift and average quadrupole splitting, are different for both compounds. Isomer shift was 0.42 for ferric benzoate and 0.38 for basic ferric benzoate; quadrupole splitting was 0.49 for the former compound and 0.81 for the last one (Figure 5).

The deconvolution of the UV-visible spectrum of the sample without zinc oxide and with the highest benzoate/iron ratio (3/1) showed the bands corresponding to α-FeOOH (380 nm to 432 nm, of variable width, and 646 nm) and the bands of α-Fe_2O_3 (290, 346, and 455 nm).[57-58] For the lowest benzoate/iron ratio (1/1) in the mixture, the bands of lepidocrosite at 385 nm and 700 nm were observed (Figure 6). The principal absorption bands of ferric benzoate were also detected together with bands of unreacted aluminum basic benzoate. Sometimes, oxide bands could also be appreciated in the FTIR spectrum, but others overlapped with benzoate bands.

The Mössbauer spectrum not only showed the iron sextet but also a central asymmetric doublet originated by a high spin ferric compound (Figure 6). This doublet was adjusted as a distribution of quadrupole splitting with the associated parameters, which were calculated and presented in Table 2. There is a great variety of substances with Mössbauer parameters at room temperature, similar to those obtained in this research. Among these compounds, lepidocrosite, super-paramagnetic goethite, and amorphous oxyhydroxides could be found. This central quadrupolar doublet was finally assigned to a hydrated ferric benzoate ($FeB_{3-x}OH_x \cdot nH_2O$) due to the similitude of Mössbauer parameters with the values encountered for the synthesized ferric basic benzoate (Table 2). These parameters are different from those obtained for the mono-dentate $Fe(C_7H_5O_2)_3$, which has an isomer shift equal to 0.40 and a quadrupole splitting of 0.60 mms^{-1}.[61]

Neither oxides nor iron oxyhydroxides were detected in the mixture containing zinc oxide. The UV-visible spectrum only showed the bands of aluminum basic benzoate, although some ferric basic benzoate could be formed. The Mössbauer spectra consisted only in the sextet of iron, thus denoting the inhibition of the corrosion reaction because this sextet (with its proper Mössbauer parameters) is characteristic of uncorroded metallic iron.[56,61] For other different iron compounds, the Mössbauer spectra change and doublets, singlets, etc., would appear.

The foregoing discussion pointed out that corrosion products could be identified easily by UV-visible spectroscopy. For this reason, the qualitative analysis of the protective layer, under the paint film described later, was carried out by this technique only.

Evaluation of Coated Steel via Accelerated Tests

The solventborne epoxy paint (paint 1) exhibited a satisfactory behavior in the salt spray chamber up to 1,770 h while waterborne epoxy (paint 3) underwent, successfully, 4,000 h of exposure (Table 3). The performance of tested paints is considered satisfactory, in current practice, when it undergoes at least 500 h of exposure with a good qualification. The behavior of alkyd paint (paint 2) was much more modest, and the panel must be retired from the chamber after 620 h of exposure (qualification 6). Blistering in the salt spray test was more important for the solvent-based epoxy paint than for the waterborne one. The former developed blisters after 620 h of exposure, which did not increase in size but in surface density during the rest of the test period. The later coating blistered after 1,580 h with smaller blisters and lower surface density. The alkyd paint did not blister during their short stay in the chamber.

Both epoxy paints maintained a very good degree of adhesion (4B) during 1,300 h. The fact that the anticorrosive protection was maintained, in spite of

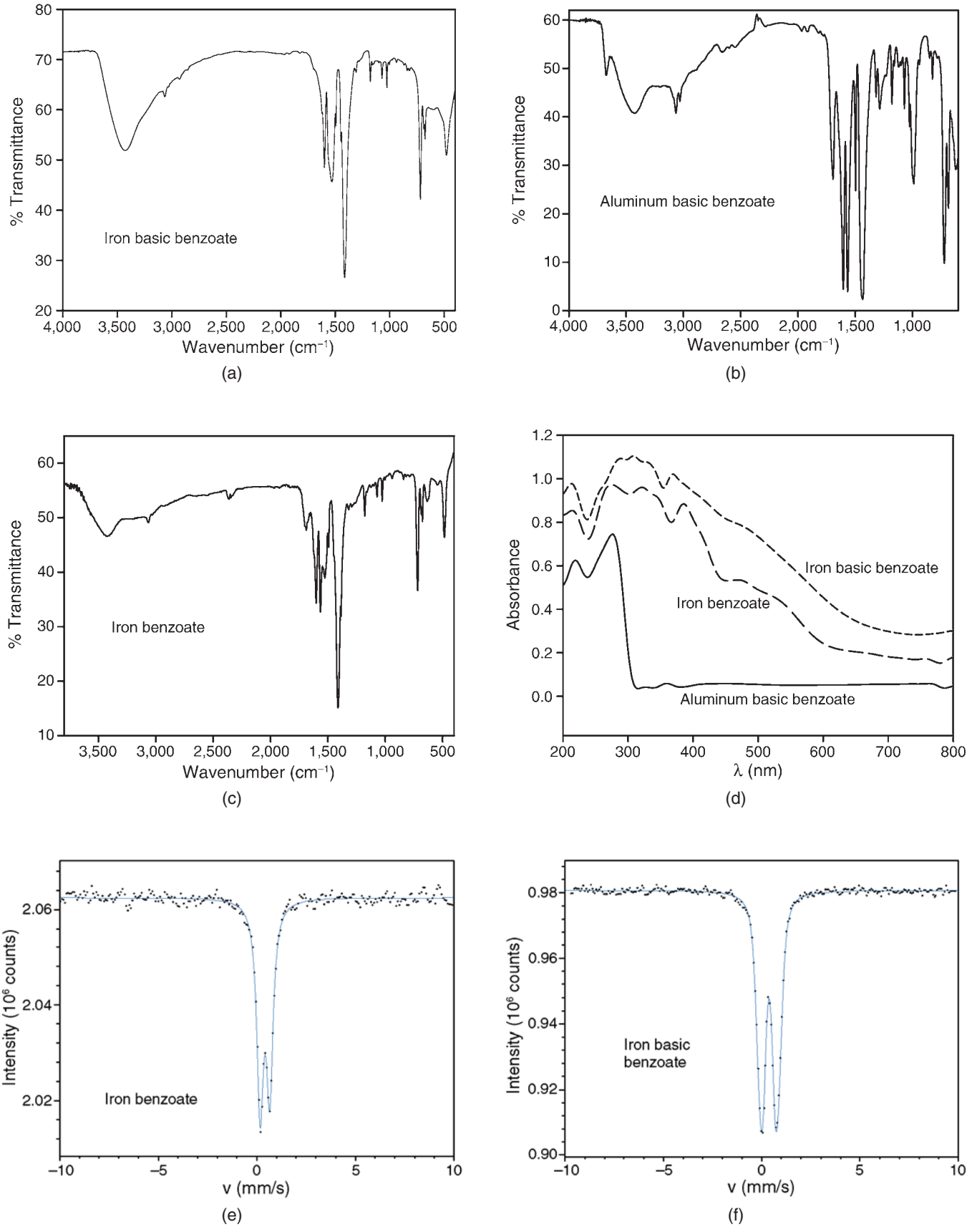

FIGURE 5. *Spectra of aluminum basic benzoate and ferric benzoates: (a), (b), (c) FTIR; (d) UV-visible diffuse reflectance; (e), (f) Mössbauer.*

the loss of adhesion, is a direct consequence of the inhibitive properties of aluminum basic benzoate. The alkyd paint presented a low adhesion value from the very beginning of the test, and the bonding forces at the paint/metal interface disappeared after 350 h of exposure (Table 4).

The anticorrosive behavior of epoxy paints in the humidity chamber was very satisfactory up to 3,150 h of exposure (qualification 7). No corrosion signs were detected during the first 1,580 h of exposure. The solventborne epoxy paint developed blisters of smaller size and lower surface density, from 1,150 h while the alkyd paint blistered after 480 h, although they did not change in size and did not increased in surface density. As expected, due to the nature of the binder, the waterborne paint developed blisters from the beginning of the test period, which increased in size and surface density as time elapsed. The resistance of alkyd paints to rusting was higher than in the salt spray test as a consequence of the lower aggressiveness of the atmosphere of this chamber (Table 5).

The anticorrosive behavior of epoxy paints formulated with this pigment exhibited similar features to the performance of paints pigmented with zinc phosphate, which was reported elsewhere.[62]

The surface morphology of steel panels was studied using SEM, after removing the organic coating with suitable solvents. Xylene was used for softening the paint film that finally was removed with THF (tetrahydrofuran [C_4H_8O]) and/or 1-methyl-2-pyrrolidinone (C_5H_9NO). The predominant morphology was an amorphous layer constituted, principally, by different iron compounds (Figure 7[a]). Sometimes, distinctive morphologies can be located at certain places on the surface. In the case of the waterborne paint, a compact and brittle layer was observed together with some formations rich in aluminum and silicon with different Si:Al:Fe ratios. This formation could be the result of the reaction of iron oxides with talc.

In all cases the concentration of carbon oscillated between 7.6% and 35.1%; the source of C was aluminum basic benzoate. The amount of iron (4.1 to 50.5) and aluminum (1.9 to 4.0) encountered using EDAX analysis suggested that aluminum basic benzoate was partially transformed into ferric benzoate. It was very difficult to distinguish the morphology of ferric benzoate and aluminum basic benzoate (Figure 7[b]).

The analysis of the layer formed under the alkyd paint was in accordance with its behavior in the salt spray chamber. As an average, the layer resulted enriched in iron content (~64.9%) and depleted in the other elements, including carbon. The oxide layer had many pores and, as a consequence, poor protective properties (Figure 7[c]). Deleterious oxide formations were detected, which appeared as dark oxide spots of globular morphology (Figure 7[d]).

The UV-visible diffuse reflectance spectra of uncoated steel panels, exposed to the saline chamber,

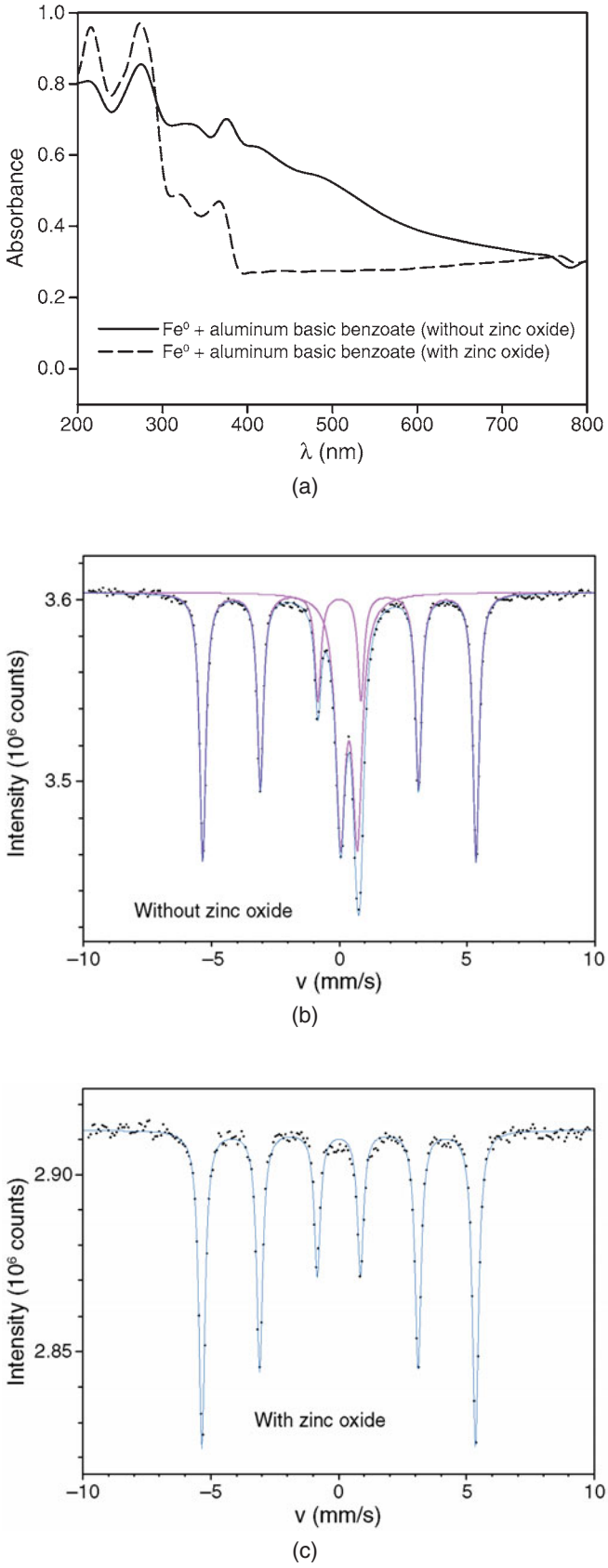

FIGURE 6. *Spectra of the products obtained from the iron/aluminum basic benzoate mix: (a) UV-visible diffuse reflectance; (b), (c) Mössbauer.*

TABLE 2

Mössbauer Parameters at Room Temperature Corresponding to the Reaction Products in a Mixture of Aluminum Basic Benzoate and Iron Powder, Without Zinc Oxide

Sample	<CS> (mm/s)	<|Δ|> (mm/s)	$\sigma_{\|\Delta\|}$ (mm/s)	Γ (mm/s)	A (%)	χ^2_{red}
Ferric benzoate	0.42	0.49	—	0.20	100.0	0.414
Iron basic benzoate	0.38	0.81	0.28	—	100.0	0.578
M1	0.40	0.80	0.37	—	26.9	0.653
M2	0.38	0.72	0.35	—	38.2	0.737

<CS>: isomer shift with respect to α-Fe.
<|Δ|>: average quadrupolar splitting.
σ: Gaussian width (standard deviation) of the quadrupolar site.
Γ: Lorentzian width of the crystalline site.
A: site contribution to the whole spectral area.
M1: molar ratio: basic aluminum benzoate/iron: 3/1.
M2: molar ratio: basic aluminum benzoate/iron: 1/1.

TABLE 3

Rusting[A] (ASTM D610) and Blistering[B] (ASTM D714) Degrees of the Painted Panels Exposed to the Salt Spray Chamber (ASTM B117)

Time (h)	Paint 1 Rusting-Blistering	Paint 2 Rusting-Blistering	Paint 3 Rusting-Blistering
120	10-10	8-10	10-10
310	9-10	7-10	10-10
620	9-6F	6-10	10-10
770	9-6F	Panels were	10-10
980	9-6F	removed from	10-10
1,150	8-6F	chamber	10-10
1,400	8-6F		10-10
1,580	8-6M		10-10
1,770	8-6M		9-10
2,500	6-6M		9-8F
3,600	Panels were		8-8F
4,000	removed		7-8F
4,200	from chamber		6-8F

[A]Rusting degree (ASTM D610)

Rust grade	10	9	8	7	6	5	4	3	2	1
Rusted area (%)	No rusted	0.03	0.1	0.3	1	3	10	16	33	50

[B]Blistering degree (ASTM D714)

Frequency	Dense, D	Medium Dense, MD	Medium, M	Few, F
Size	10	8	6, 4	2
Comments	No blistering	Smaller size blister easily seen with unaided eye	Progressively larger sizes	

are shown in Figure 8. The protective coating formed just below the solvent-based epoxy coating was constituted by δ-FeOOH with bands at 220 nm and 263 nm to 412 nm (flat maximum), α-FeOOH (goethite) with absorption bands at 380 nm to 342 nm (variable width), 451 nm (shoulder), and 646 nm, and α-Fe_2O_3 with bands located at 220, 292, 346, and 455 nm.[57-59,63] Lepidocrosite was not detected in the analyzed sample. Ferric benzoate and ferric basic benzoate were also formed, since it could be deduced by their absorption bands between 300 nm and 400 nm where aluminum basic benzoate does not absorb radiation. The protective layer formed under the alkyd coating was composed mainly of α-FeOOH and α-Fe_2O_3 together with ferric benzoates. The protective coating formed under the waterborne paint was also formed by alpha oxides and oxyhydroxides, as in the case of the alkyd coating, although only the presence of ferric benzoate was detected.

Electrochemical Impedance Spectroscopy

Equivalent Circuits — Impedance spectra provide useful information concerning the evolution of both the organic coating protective properties and the kinetics of the underlying steel corrosion process, as a function of the immersion time in the selected electro-

TABLE 4

Wet Adhesion Test[C] (ASTM D3359) of Painted Panels as a Function of the Exposure Time to the Salt Spray Chamber (ASTM B117)

Time (h)	0	48	120	350	640	956	1,300	1,800	2,400
Paint 1	5 B	5 B	5 B	4 B	4 B	4 B	4 B	3 B	3B
Paint 2	3 B	3 B	2 B	1 B	0 B	Panels were removed from chamber			
Paint 3	5 B	5 B	5 B	5 B	4 B	4 B	4 B	3 B	3 B

[C]Tape-test method B (ASTM D3359-97)

Classification	5 B	4 B	3 B	2 B	1 B	0 B
Removed area (%)	0	<5	5-15	15-35	35-65	>65

TABLE 5

Rusting (ASTM D610) and Blistering (ASTM D714) Degrees of the Painted Panels Exposed to the Humidity Chamber (ASTM B2247)

Time (h)	Paint 1 Rusting-Blistering	Paint 2 Rusting-Blistering	Paint 3 Rusting-Blistering
96	10-10	10-10	10-8F
480	10-10	10-10	10-6F
770	10-10	10-8F	10-6F
980	10-10	10-8M	10-6F
1,150	10-8F	9-8MD	10-6F
1,400	10-8F	8-8MD	10-6M
1,580	10-8F	7-8MD	10-6M
1,770	10-8F	6-8D	9-6M
2,130	9-8F	Panels were	9-6M
2,650	8-8F	removed from	8-6MD
2,890	8-8F	chamber	8-6MD
3,150	7-8F		7-6MD
3,600			6-6MD

lyte. Many processes such as the dynamic nature of the membrane barrier, the pigments' anticorrosive action, changes in the disbonded area, etc., are responsible of the variations of the coated steel/electrolyte impedance. The point of view adopted in this paper was that of Amirudin and Thierry[64] in the sense that visual observation of the spectra could not indicate the exact number of time constants involved in the degradation of the organic coating subjected to a corrosive environment. The number of these constants must be determined by data analysis rather than by the visual observation of the spectra. Fortunately, an appropriate equivalent circuit has been proposed to describe the behavior of the painted metals, as shown in Figure 9; these circuits were discussed previously by several authors.[64-69] Experimental impedance data are usually fitted with nonlinear least-squares algorithms, involving the transfer function derived from the equivalent circuit models, to obtain circuit parameters.[70-73]

The impedance of a high-quality, nondefective organic coating is that of a dielectric capacitor with a frequency dependence expressed by the following equation:

$$Zc = -j/wC \quad (12)$$

However, as the coating degrades, an in-phase component develops as a result of shorting the organic coating capacitance with a parallel resistor. This resistor represents the development of ionic conducting paths that might occur through microscopic pores or virtual pores defined by low cross-linking regions in the polymer with concomitant high ionic transport. This model has essentially been proposed by Brasher and Nurse,[73] Kendig and Leidheiser,[74-75] Kendig and Scully,[66] Mansfeld and Kendig,[76] and Beaunier, et al.[77] Thus, R represents the electrolyte resistance between the reference and working (coated steel) electrodes, R_1 is the resistance to the ionic flux through paths short-circuiting the paint film, and C_1 is the dielectric capacitance of the intact part of the same film, as illustrated in Figure 9(a).

Once the permeating and corrosion-inducing chemicals (water, oxygen, and ionic species) reach the electrochemically active areas of the substrate, particularly the bottom of the paint film pores, metallic corrosion takes place and its associated parameters, the double-layer capacitance (C_2) and the charge-transfer resistance (R_2), can be obtained from the fitting procedure. It is important to remark that R_2 and C_2 values vary inversely and directly, respectively, and with the size of the attacked metallic area.

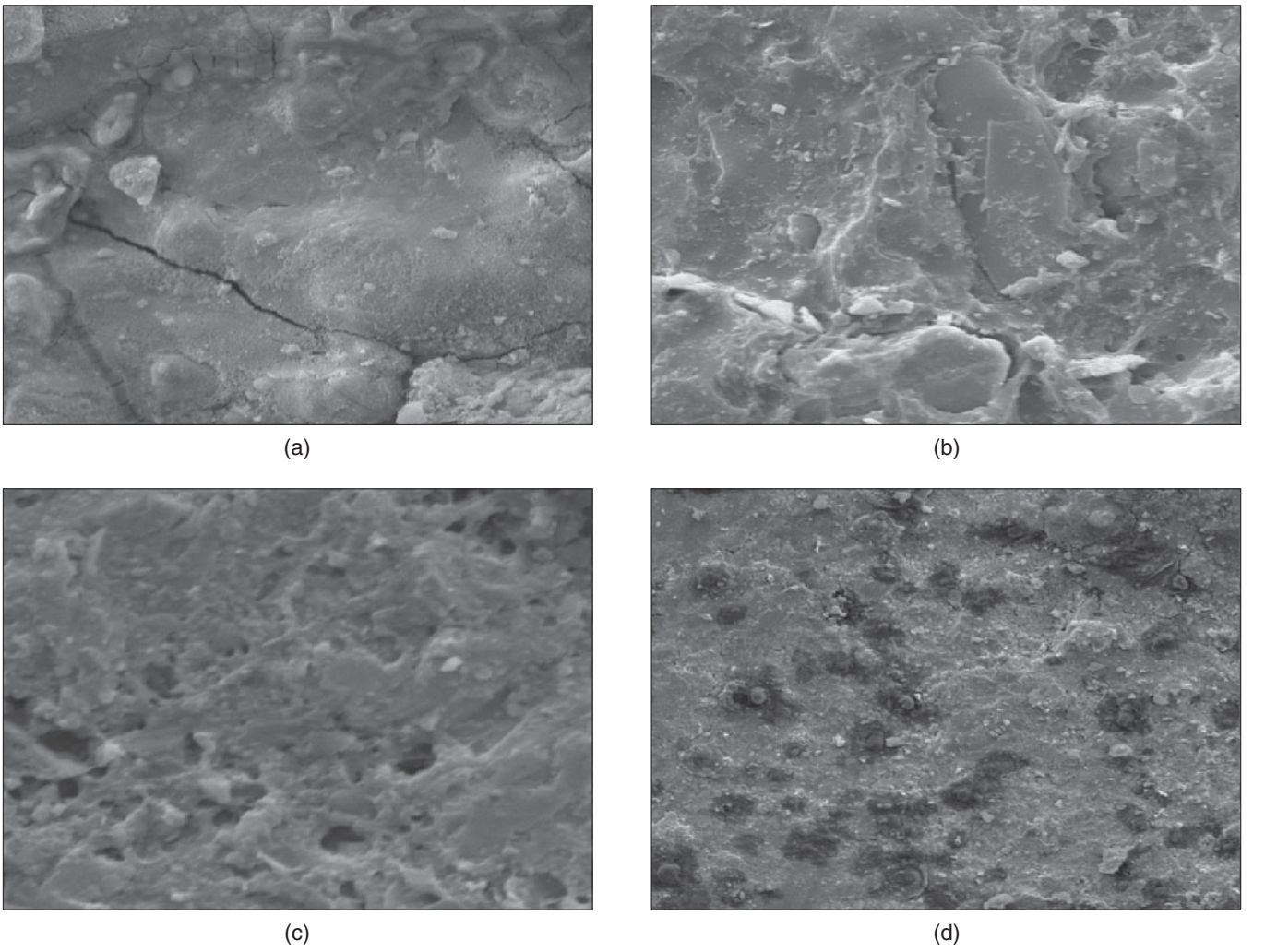

FIGURE 7. *SEM micrographs of the steel surface after removing the different coatings on panels exposed to the salt spray chamber (ASTM B117). Magnification: (a), (b) 1,000X; (c) 2,000X; and (d) 250X.*

There is almost a unanimous opinion that a polymer-coated metal is represented by the circuit in Figure 9(c) when water penetrates the coating and reaches the metal. It is also agreed that the general impedance may include the Zd, the mass-transfer (Warburg) impedance.[64]

Sometimes, when the strength of the bonding forces at the paint/substrate interface are affected (e.g., by wet adhesion), facilitating lateral diffusion of the electrolyte, other processes under and/or within the intact parts of the coating could be graphically and/or numerically separated,[78] causing the appearance of additional time constants (R_3C_3).

Distortions observed in these resistive-capacitive contributions indicate a deviation from the theoretical models due to either lateral penetration of the electrolyte at the steel/paint interface (usually started at the base of intrinsic or artificial coating defects), underlying steel surface heterogeneity (topological, chemical composition, surface energy), and/or diffusional processes that could take place along the test.[79-80] Since all these factors cause the impedance/frequency relationship to be nonlinear, they are taken into consideration by replacing the capacitive components (C_i) of the equivalent circuit transfer function by the corresponding constant phase element Q_i (CPE), thus obtaining a better fit of data.[64,81] The CPE is defined by the following equation:[82]

$$Z = \frac{(j\omega)^{-n}}{Y_0} \qquad (13)$$

where Z is the impedance of the CPE ($Z = Z' + Z''$), (Ω); j is the imaginary number ($j^2 = {}^{-1}$); ω is the angular frequency (rad); n is the CPE power ($n = \alpha/[\pi/2]$), (dimensionless); α is the constant phase angle of the CPE, (rad); and Y_0 is the part of the CPE independent of the frequency, ($s^{\alpha}\Omega^{-1}$).

The accuracy of the fitting procedure was measured by the χ^2 parameter obtained from the differ-

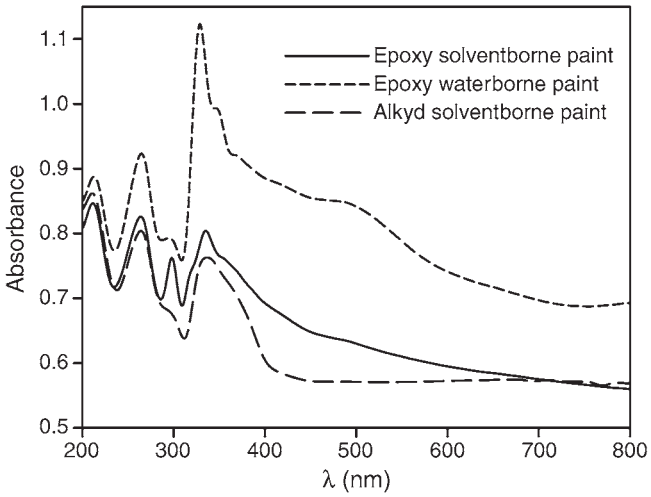

FIGURE 8. *UV-visible diffuse reflectance spectra of the steel surface of coated panels exposed to the salt spray, after paint removal by suitable solvents.*

ence between experimental and fitted data. The most probable circuit was selected providing that $\chi^2 < 10^{-4}$. In the present work, the fitting process was performed using the phase constant element Q_i.

Electrochemical Impedance Spectroscopy Discussion — The corrosion potential of steel panels coated with the solventborne epoxy paint was displaced to more positive values with respect to the other panels (Figure 10). The influence of the electrolyte was perceived at the end of the immersion period when the corrosion potential in 0.5 M $NaClO_4$ was almost 200 mV more positive than in 3% NaCl. Moreover, the panel submerged in 3% NaCl exhibited a broad peak pointing to positive values, which may be attributed to the formation of a passive layer under the paint film at early times. This process was more pronounced than in the case of the panel in 0.5 M $NaClO_4$ and was thought to be due to the aggressiveness of the electrolyte. Good protection was achieved with this paint during, at least, 4 months and it could be attributed to the slow penetration of water as it could be expected in an epoxy coating, together with the inhibitive action of aluminum basic benzoate.

The alkyd paints, which are less resistant to water permeation, deteriorated in a much shorter period of time, and steel corrosion potential moved toward negative values in less than a week of immersion (Figure 10). As a consequence, the incidence of the corrosion process became appreciable and the test must be discontinued.

Waterborne coatings had an intermediate behavior between both types of solventborne paints. The evolution of corrosion potential values toward more negative values was slower than in the case of the alkyd, and the difference between both types of electrolytes could also be appreciated (Figure 10).

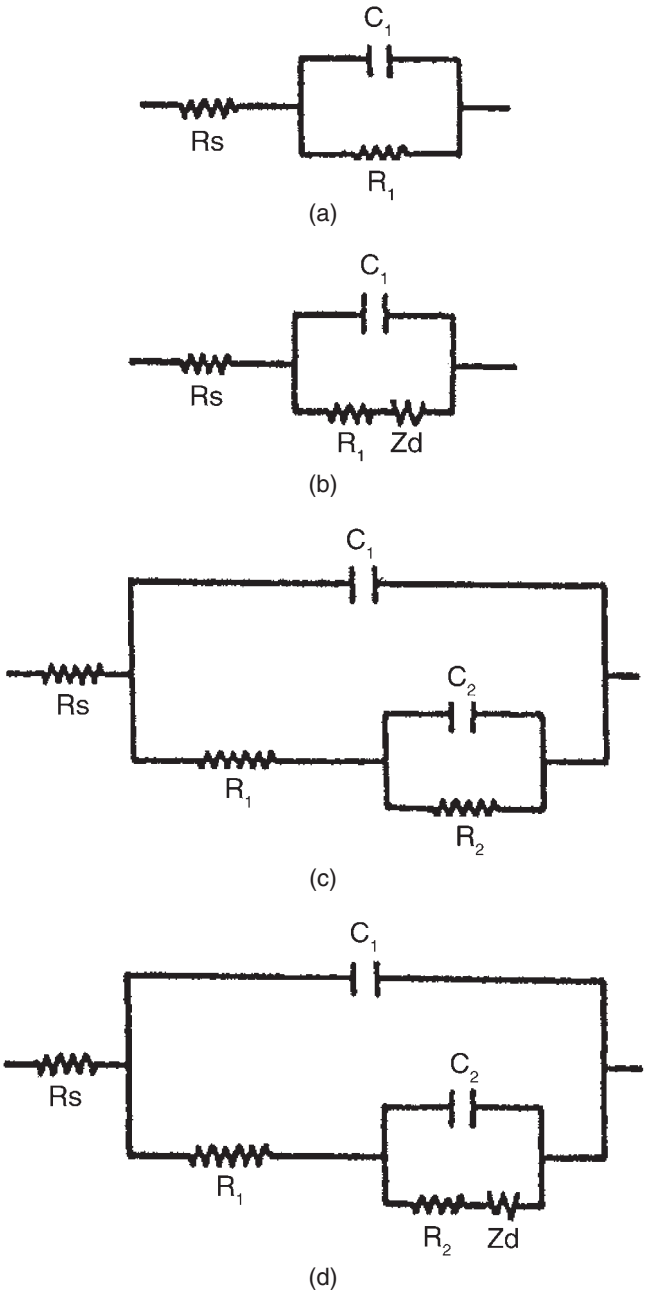

FIGURE 9. *The different equivalent circuits model the behavior of organic coatings: (a) intact coating; (b) a coating with a diffusion process across it; (c) and (d) a coating where the Faradaic process associated with corrosion started.*

The examination of Bode's plot corresponding to paint 1 (solventborne epoxy coating, Figures 11 and 12), in both electrolytes, revealed that the coating showed a behavior that was predominantly capacitive during, at least, three weeks of immersion. It is also clear that more than one time constant is involved in the coating degradation process. The most sensitive parameter to infer the existence of more than one time constant is the frequency dependence of the phase angle. As it can be seen in Figures 11 and 12,

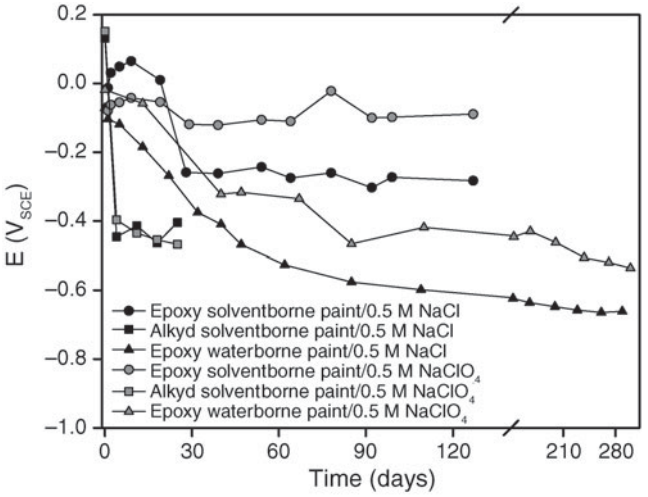

FIGURE 10. *Corrosion potential of coated steel in 0.5 M $NaClO_4$ and 3% NaCl.*

the value of the phase angle, close to 90°, and more or less independent of the frequency at the end of the first hour of immersion, is indicative of an almost pure capacitive (i.e., dielectric) response. However, at higher exposure times, it diminishes as the frequency does and approaches 0° at low frequencies, thus indicating a mixed capacitive-resistive behavior.

The analysis of Bode's plot of the alkyd paint (paint 2), in both electrolytes (Figures 13 and 14), show that the phase angle was close to 90° during the first day of immersion, thus indicating a capacitive behavior originated in an almost intact coating. The deviation from a purely capacitive behavior is more evident in a chloride medium (Figure 14). Beyond the first day of immersion, the existence of more than one time constant became evident as well as an important decrease in the impedance of the steel/coating system. A recovery of the barrier properties was noticed in a perchlorate medium when 96 days of immersion had elapsed. This behavior could be originated by pore blocking by corrosion products and was accompanied by the corresponding increase in the phase angle value.

Bode plots obtained with the waterborne coating, in both electrolytes (Figures 15 and 16), pointed out the existence of more than one time constant. The behavior, as in the other cases, was predominantly capacitive during the first day of immersion. The impedance modulus was higher than 10^6 Ω during the test period and increased as time elapsed, probably due to pore blocking by corrosion products.

Since more than one time constant was involved in all impedance spectra, experimental data were fitted with the equivalent circuits presented in Figure 9, as was suggested by Amirudin and Thierry.[64] The result of the fitting procedure is recorded in Figures 17 through 19 and represented as the variation of the R_iQ_i values as a function of time.

All of the paints showed a high barrier effect ($R_1 > 10^9$ Ω·cm^{-2}), which was lost after a few days of immersion. However, epoxy paints maintained a residual barrier effect ($R_1 > 10^9$ Ω·cm^{-2}) during almost all the test periods (Figure 17). The permeation of the electrolyte through coating pores of the solventborne epoxy paint caused it to lose its barrier properties after 80 days of immersion. The plot of R_1 vs. time for epoxy paints showed an oscillating behavior due to pore blocking with corrosion products, which temporarily

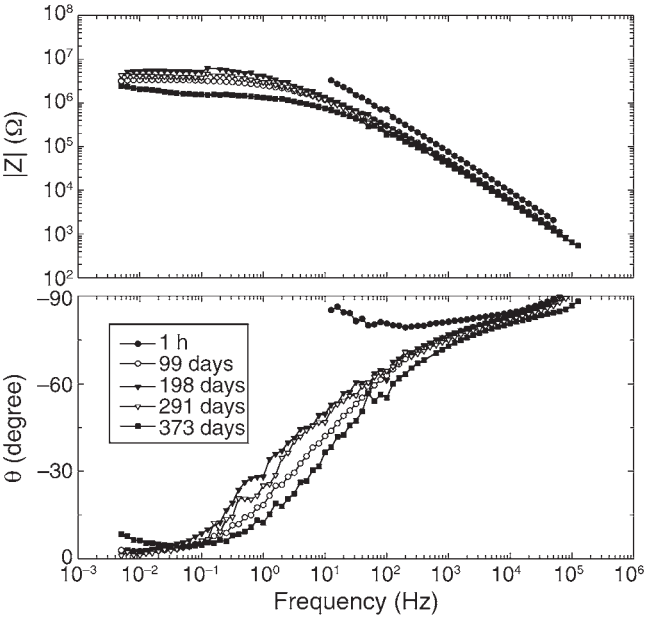

FIGURE 11. *Bode plots at different exposure times for paint 1 in 0.5 M $NaClO_4$.*

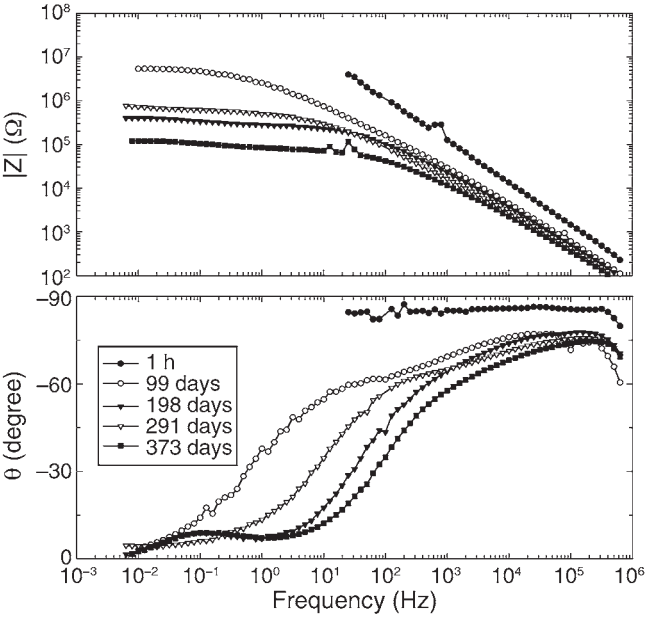

FIGURE 12. *Bode plots at different exposure times for paint 1 in 3% NaCl.*

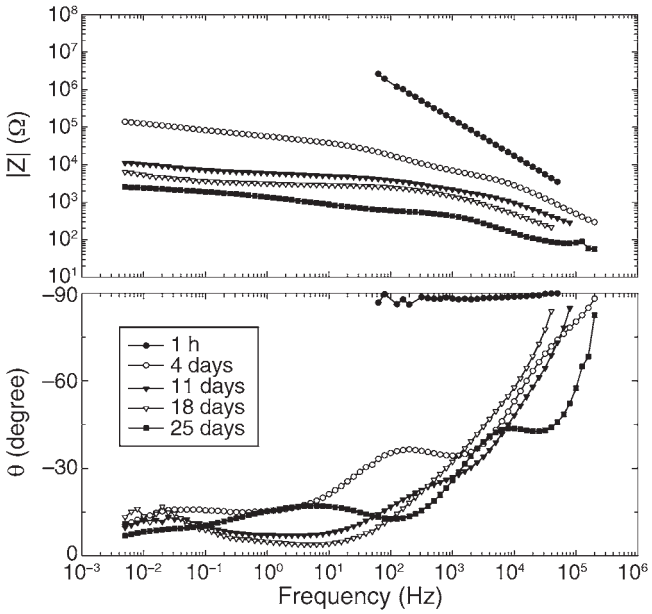

FIGURE 13. *Bode plots at different exposure times for paint 2 in 0.5 M $NaClO_4$.*

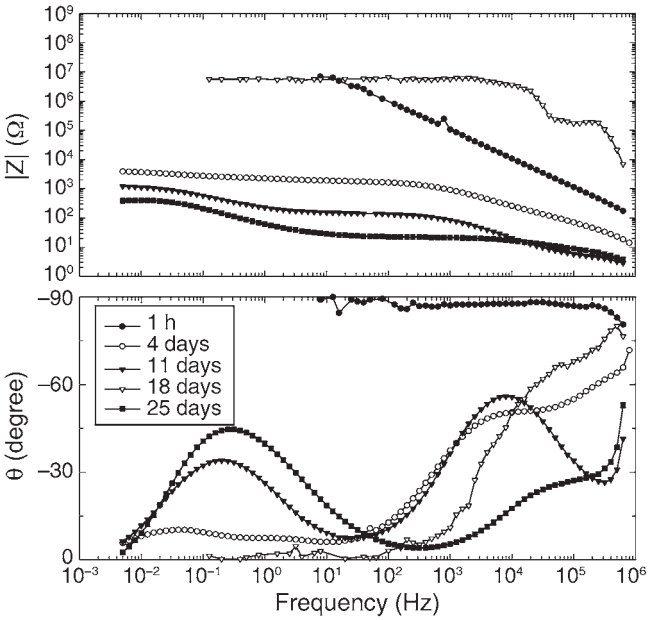

FIGURE 14. *Bode plots at different exposure times for paint 2 in 3% NaCl.*

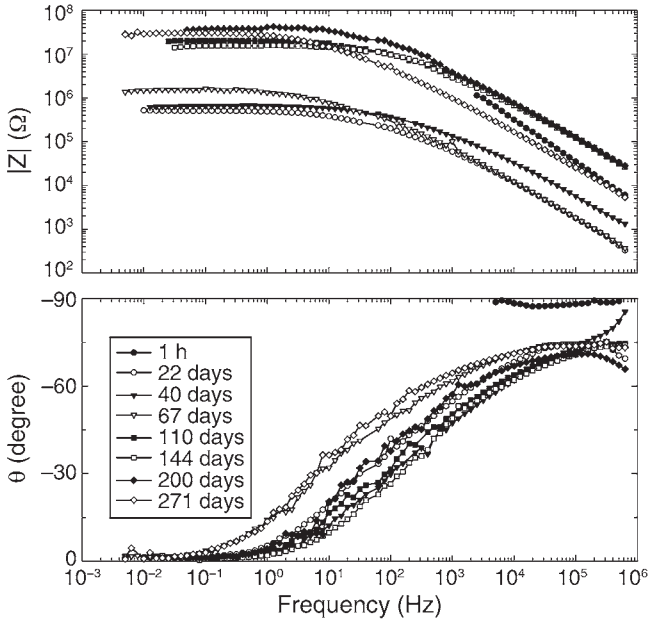

FIGURE 15. *Bode plots at different exposure times for paint 3 in 0.5 M $NaClO_4$.*

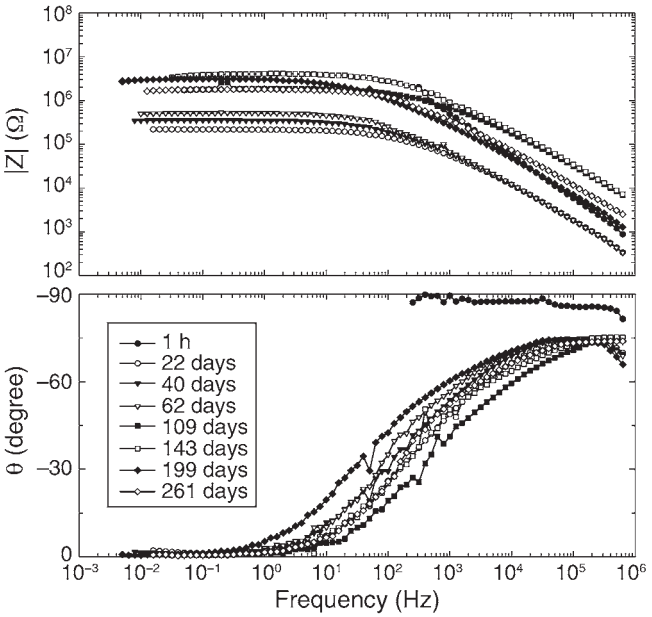

FIGURE 16. *Bode plots at different exposure times for paint 3 in 3% NaCl.*

improved substrate protection. Except for the alkyd paints, capacitance values corresponded to paint films with very little degree of degradation.[83-85]

The parameters associated with the Faradaic process, R_2, Q_2 (Figure 18), showed an important inhibition of the corrosion process in the case of epoxy paints in both electrolytes. The relaxation of the corrosion process was appreciated from early times. Waterborne epoxy paint showed an improved behavior at the end of the test period probably due to the chemisorption of the binder on the steel substrate.[62] The charge-transfer resistance of alkyd paints was some orders of magnitude lower than for epoxies, thus revealing a significant progress of the corrosion process.

The capacitance of the electrochemical double layer was, as an average, lower than 10^{-8} F·cm^{-2}; it

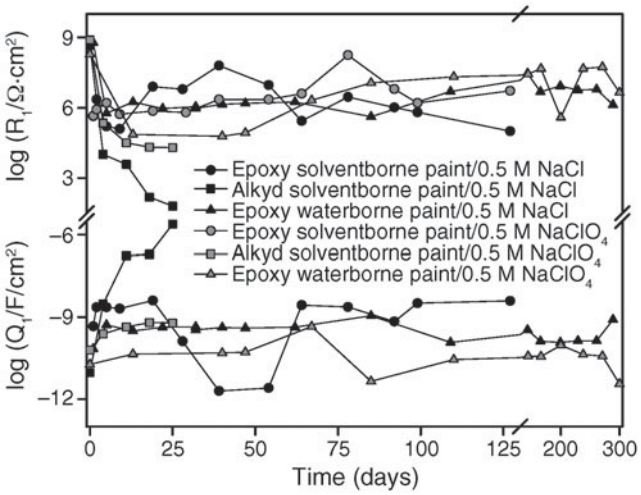

FIGURE 17. *Fitting parameters, R_1 and Q_1, for the different coatings, as a function of the immersion time in 0.5 M $NaClO_4$ and 3% NaCl.*

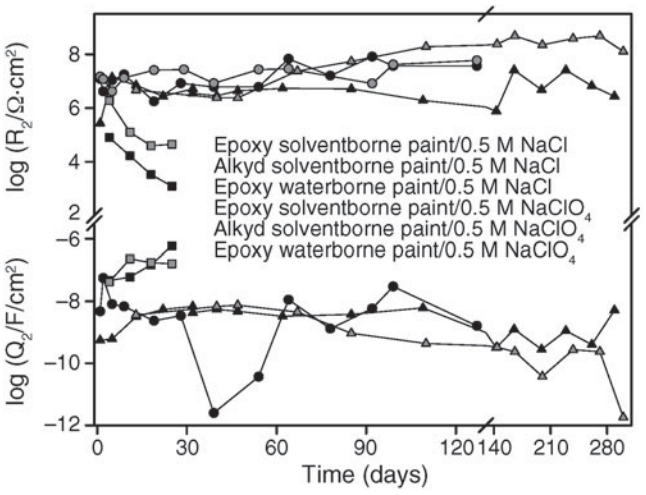

FIGURE 18. *Fitting parameters, R_2 and Q_2, for the different coatings, as a function of the immersion time in 0.5 M $NaClO_4$ and 3% NaCl.*

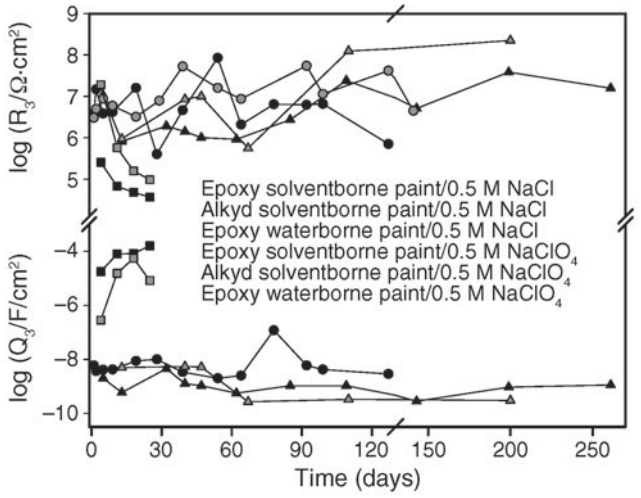

FIGURE 19. *Fitting parameters, R_3 and Q_3, for the different coatings, as a function of the immersion time in 0.5 M $NaClO_4$ and 3% NaCl.*

did not increase as time elapsed and, on the contrary, showed a certain tendency to decrease. This last fact would reveal that active sites were passivated by the pigment. Capacitance values for the alkyd paint showed an increasing behavior during all the test periods as a consequence of the deterioration process of the coating.

The corrosion under delaminated areas was also evident from the beginning of the test period (Figure 19) because it could be deduced from the existence of another time constant (R_3, Q_3). However, except for the alkyd paint, the corrosion of the substrate was strongly inhibited by aluminum basic benzoate. The capacitance values are rather low and tended to decrease a little, pointing out the fact that the delaminated area was small and passivated during the test period.

CONCLUSIONS

❖ Aluminum basic benzoate could be precipitated adequately from sodium benzoate solution using aluminum nitrate. The pigment solubility was adequate to formulate anticorrosive paints.

❖ The electrochemical tests performed using pigment suspensions confirmed the anticorrosive properties of the inhibitor.

❖ The protective layer formed on steel could be formed by iron oxides or oxyhydroxides as well as ferric benzoates.

❖ Electrochemical testing showed that aluminum basic benzoate must be used together with zinc oxide to neutralize the hydrolytic acidity of the pigment.

❖ Accelerated tests showed that aluminum basic benzoate also performed satisfactorily in epoxy paints. Its anticorrosive behavior is equal or even better than zinc phosphate, except for alkyd paints.

❖ Electrochemical tests showed that the pigment generated very high charge-transfer resistance values, which were responsible of the protection afforded by the paints. The barrier properties were of much less importance.

ACKNOWLEDGMENTS

The authors are grateful to CONICET (Consejo Nacional de Investigaciones Científicas y Técnicas), CICPBA (Comisión de Investigaciones Científicas de la Provincia de Buenos Aires), and UNLP (Universidad Nacional de La Plata) for their sponsorship of this research. G. Blustein also thanks F.V. Vetere for advice on analytical topics.

REFERENCES

1. D. Eurof Davies, G.J.M. Slaiman, Corros. Sci. 11 (1971): p. 671.

2. Q.J.M. Slaiman, D. Eurof Davies, Corros. Sci. 11 (1971): p. 683.
3. D. Eurof Davies, Q.J.M. Slaiman, Corros. Sci. 13 (1973): p. 891.
4. V.S. Muralidharan, R. Sethuraman, S. Krishnamoorthy, Bull. Electrochem. 4 (1988): p. 705.
5. D.S. Azambuja, L.R. Holzle, I.L. Muller, C.M.S. Piatnicki, Corros. Sci. 41 (1999): p. 2,083.
6. M. Yamaguchi, H. Nishihara, K. Aramaki, Corros. Sci. 36 (1994): p. 241.
7. M. Ergun, Y.S. Turan, Corros. Sci. 32 (1991): p. 1,137.
8. V. Otieno-Alego, G.A. Hope, H.J. Flitt, G.A. Cash, D.P. Schweinsberg, Corros. Sci. 33 (1992): p. 1,719.
9. R. Kahraman, A.A. Al-Mathami, H. Saricimen, N. Abbas, S.U. Arman, Anticorros. Methods Mater. 49 (2002): p. 346.
10. P. Argawal, D. Landolt, Corros. Sci. 4/5 (1998): p. 673.
11. R. Kahraman, J. Mater. Eng. Perform. 11 (2002): p. 46.
12. K. Takahashi, J.A. Bardwell, B. MacDougall, M.J. Graham, Electrochim. Acta 37 (1992): p. 489.
13. J.R. Culleré, M. Lluveras, Rev. Iberoam. Corros. Prot. (1983): p. 225.
14. G. Bondietti, J. Sinniger, W. Stumm, Colloids Surf. A 79 (1993): p. 157.
15. R. Kahraman, H. Saricimen, Al-Zahrani, S. Al-Dulaijan, J. Mater. Eng. Perform. 12 (2003): p. 524.
16. O. Lahodny-Šarc, F. Kapor, Mater. Sci. Forum (1998): p. 1,205.
17. G. Blustein, J. Rodríguez, C.F. Zinola, R. Romagnoli, Corros. Sci. 47 (2005): p. 369.
18. P.N.S. Yadav, A.K. Singh, R. Wadhwani, Corrosion 55 (1999): p. 937.
19. A. Raspini, Corrosion 49 (1993): p. 821.
20. A.K. Mohamed, S.A. Abd El-Maksoud, A.S. Fonda, Port. Electrochim. Acta 15 (1997): p. 27.
21. S. Zor, Turk J. Chem. 26 (2002): p. 403.
22. W.J. Rudd, J.R. Scully, Corros. Sci. 20 (1980): p. 611.
23. K. Aramaki, Corros. Sci. 43 (2001): p. 1,985.
24. S.M. Abd El Haleem, A.A. Abdel Fattah, Surf. Coat. Technol. 29 (1986): p. 41.
25. S.N. Mostafa, M.Y. Mourand, S.A. Seliman, J. Electroanal. Chem. 130 (1981): p. 221.
26. G. Blustein, C.F. Zinola, J. Colloid Interf. Sci. 278 (2004): p. 393.
27. P. Kern, D. Landolt, Electrochim. Acta 47 (2001): p. 589.
28. C. Monticelli, A. Frignani, G. Trabanelli, Cem. Concr. Res. 30 (2000): p. 635.
29. J.M. Gaidis, Cem. Concr. Compos. 26 (2004): p. 181.
30. F. Galliano, D. Landolt, Prog. Org. Coat. 44 (2002): p. 217.
31. S.A. Hodges, W.M. Uphues, M.T. Tran, Surf. Coat. Int. 4 (1997): p. 178.
32. C.H. Simpson, Paint Coatings Ind. (1993).
33. M.A. Jackson, J. Prot. Coatings Linings (1990): p. 54-64.
34. A. Kalendová, Prog. Org. Coat. 44 (2002): p. 201.
35. Technical sheet, Halox® Flash-X330 Halox Flash Rust Inhibitors.
36. G. Pollano, A. Lurier, Paint Coatings Ind. 5/6 (1987).
37. I. Chet, P. Asketh, R. Mitchell, Appl. Microbiol. 30 (1975): p. 1,043.
38. M. Stupak, M. García, M.C. Pérez, Int. Biodeterior. Biodegrad. 52 (2003): p. 49.
39. ASTM D1475-98(2003), "Standard Test Method for Density of Liquid Coatings, Inks, and Related Products," in Annual Book of ASTM Standards (West Conshohocken, PA: ASTM International, 2003).
40. ASTM D281-95(2007), "Standard Test Method for Oil Absorption of Pigments by Spatula Rub-Out," in Annual Book of ASTM Standards (West Conshohocken, PA: ASTM International, 2007).
41. Z. Szklarska-Smialowska, R.W. Staehle, J. Electrochem. Soc. 121 (1974): p. 1,393.
42. M.C. Deyá, R. Romagnoli, B. del Amo, Corros. Rev. 22 (2004): p. 1.
43. A. Gerhard, A. Bittner, J. Coat. Technol. 58 (1986): p. 59.
44. A. Bittner, JCT 61 (1984): p. 114.
45. C.A. Giúdice, J.C. Benítez, V.J.D. Rascio, J. OCCA 63 (1980): p. 153.
46. S. Gee, Surf. Coat. J. 80 (1997): p. 316.
47. Sveriges Standardiseringskommission, "Rust Grades for Steel Surfaces and Preparation Grades Prior to Protective Coating," Swedish Standard, SIS 05.59.00 (1962), p. 55.
48. ASTM B117-90, "Standard Method of Salt Spray (Fog) Testing," in Annual Book of ASTM Standards (West Conshohocken, PA: ASTM International, 1990).
49. ASTM D610-95, "Standard Test Method for Evaluating Degree of Rusting on Painted Steel Surfaces," in Annual Book of ASTM Standards (West Conshohocken, PA: ASTM International, 1995).
50. ASTM D714-87, "Standard Test Method for Evaluating Degree of Blistering fo Paints," in Annual Book of ASTM Standards (West Conshohocken, PA: ASTM International, 1987).
51. ASTM D3359-02, "Standard Test Methods for Measuring Adhesion by Tape Test," in Annual Book of ASTM Standards (West Conshohocken, PA: ASTM International, 2002).
52. ASTM D2247-02, "Standard Practice for Testing Water Resistance of Coatings in 100% Relative Humidity," in Annual Book of ASTM Standards (West Conshohocken, PA: ASTM International, 2002).
53. B.A. Boukamp, "Equivalent Circuit (Equivcrt.pas)," Report CT88/265/128, CT89/214/128, University of Twente, The Netherlands, 1989.
54. C. Wilson, D. Wilson, Comprehensive Analytical Chemistry (Amsterdam, The Netherlands: Elsevier Publishing Company, 1960), p. 152-153.
55. R.B. Fischer, D.G. Peters, Quantitative Chemical Analysis (Mexico: W.B. Saunders Co., 1968), p. 260-266.
56. G. Blustein, "Metallic Benzoates as Anticorrosive Pigments, Synthesis and Characterization," in Development of Metallic Benzoates-Based Inhibitors for Steel Anticorrosive Protection (Thesis, National University of La Plata, La Plata, Argentina, 2005), ch. 3.
57. G. Larramona, C. Gutiérrez, J. Electrochem. Soc. 136 (1989): p. 2,171.
58. R.V. Morris, H.V. Lauer, C.A. Lawson, E.K. Gibson, Jr., G.A. Nace, C. Stewart, J. Geophys. Res. 90 (1985): p. 3,126.
59. R.G.J. Strens, B.J. Wood, Mineral. Mag. 43 (1979): p. 347.
60. K. Hirayama, Handbook of Ultraviolet and Visible Absorption Spectra of Organic Compounds (New York, NY: Plenum Press, 1967), p. 184.
61. P.S. Bassi, B.S. Randhawa, H.S. Jamwal, Termochim. Acta 69 (1983): p. 367.
62. G. Blustein, M.C. Deyá, R. Romagnoli, B. del Amo, Appl. Surf. Sci. 252 (2005): p. 1,386.
63. S.P. Tandon, J.P. Gupta, Spectrosc. Lett. 3 (1970): p. 297.
64. A. Amirudin, D. Thierry, Br. Corros. J. 30, 2 (1995): p. 128-134.
65. F. Mansfeld, Corrosion 36, 5 (1981): p. 301-307.
66. M. Kendig, J. Scully, Corrosion 46, 1 (1990): p. 22-29.
67. T. Szauer, Prog. Org. Coat. 10 (1982): p. 171-183.
68. A. Miszczyk, H. Szalinska, Prog. Org. Coat. 25 (1995): p. 357-363.
69. O. Ferraz, E. Cavalcanti, A.R. Di Sarli, Corros. Sci. 37, 8 (1995): p. 1,267.
70. P.R. Seré, D.M. Santágata, C.I. Elsner, A.R. Di Sarli, Surf. Coat. Int. 3 (1998): p. 128.
71. D.M. Santágata, P.R. Seré, C.I. Elsner, A.R. Di Sarli, Prog. Org. Coat. 33 (1998): p. 44.
72. P.R. Seré, A.R. Armas, C.I. Elsner, A.R. Di Sarli, Corros. Sci. 38, 6 (1996): p. 853.
73. D. Brasher, T.J. Nurse. J. Appl. Chem. 9 (1959): p. 96-105.
74. H. Leidheiser, Jr., M.W. Kendig, Corrosion 32 (1976): p. 69.
75. M.W. Kendig, H. Leidheiser, J. Electrochem. Soc. 123, 7 (1976): p. 982.
76. F. Mansfeld, M. Kendig, Electrochemical Impedance Tests for Protective Coatings, ASTM Publication STP 866, eds. C. Haynes, R. Baboian (West Conshohocken, PA: ASTM International, 1985), p. 122-142.
77. L. Beaunier, I. Epelboin, J.C. lestrade, H. Takenouti, Surf. Technol. 3 (1976): p. 237.
78. C. Gabrielli, M. Keddam, O.R. Mattos, H. Takenouti, J. Electroanal. Chem. 117 (1987): p. 813.
79. T. Szauer, A. Brandt, J. Oil Colour. Chem. Assoc. 67 (1984): p. 13.
80. D.J. Frydrych, G.C. Farrington, H.E. Townsend, Corros. Protection by Organic Coatings, vol. 87-2, eds. M.W. Kendig, H. Leidheiser, Jr. (Pennington, NJ: The Electrochemical Society, 1987), p. 240.
81. B.A. Boukamp, Report CT88/265/128, CT89/214/128, University of Twente, The Netherlands, 1989.
82. E.P.M. van Westing, G.M. Ferrari, F.M. Geenen, J.H.W van de Wit, Prog. Org. Coatings 23 (1993): p. 89.
83. T. Szauer, Prog. Org. Coat. 10 (1982): p. 171.
84. C.I. Elsner, A.R. Di Sarli, J. Braz. Chem. Soc. 5 (1994): p. 15.
85. H. Leidheiser, Prog. Org. Coat. 7 (1979): p. 70.